Plant defensin MtDef4-derived antifungal peptide with multiple modes of action and potential as a bioinspired fungicide

Meenakshi Tetorya[1*], Hui Li[1*], Arnaud Thierry Djami-Tchatchou[1], Garry W. Buchko[3], Kirk J. Czymmek[1, 2], Dilip M. Shah[1]

[1]Donald Danforth Plant Science Center, St Louis, MO. 63132, USA.

[2]Advanced Bioimaging Laboratory, Donald Danforth Plant Science Center, St Louis, Missouri 63132, USA

[3]Earth and Biological Sciences Directorate, Pacific Northwest National Laboratory, Richland, WA 99354, USA

Corresponding Author: Dilip M. Shah

(Email: dshah@danforthcenter.org)

*****These authors made equal contribution to the manuscript.

ABSTRACT

Chemical fungicides have been instrumental in protecting crops from fungal diseases. However, mounting fungal resistance to many of the single-site chemical fungicides calls for the development of new antifungal agents with novel modes of action (MoA). The sequence-divergent cysteine-rich antifungal defensins with multiple MoA are promising starting templates for design of novel peptide based fungicides. Here, we designed a set of 17-amino acid peptides containing the γ-core motif of the antifungal plant defensin MtDef4. These peptides exhibited antifungal properties different from those of MtDef4. Focused analysis of a lead peptide GMA4CG_V6 showed it had a random coil in solution with potent cation-tolerant antifungal activity against the plant fungal pathogen *Botrytis cinerea*. Its multi-site MoA involved plasma membrane permeabilization, internalization into the vacuole and cytoplasm, and binding to phosphoinositides. Topical spray-application of GMA4CG_V6 on *Nicotiana benthamiana* and tomato plants provided preventative and curative suppression of gray mold disease symptoms. Our findings open the possibility that truncated and modified defensin-derived peptides could serve as promising candidates for further development as bioinspired fungicides.

INTRODUCTION

Crop plants are under constant threat from fungal and oomycete pathogens that cause significant pre- and post-harvest economic losses worldwide and challenge food security globally[1]. This threat is increasing in severity and scale[2,3]. It is estimated that fungal and oomycete pathogens cause up to 10-23% yield losses in calorie crops[3] and postharvest losses of 10%[4]. Modern intensive agriculture depends heavily on chemical fungicides for management of fungal and oomycete diseases in commodity crops as well as high value vegetable and fruit crops[5]. Most chemical

fungicides in use today have a single biochemical target and thus are prone to resistance development by diverse and rapidly evolving fungal and oomycete strains[6]. In face of fungal resistance and unwanted side effects, some fungicides are losing their effectiveness in modern intensive monoculture cropping systems. The structurally diverse plant antifungal peptides with potent antifungal activity could potentially serve as structural templates for the design of new-generation of safe and sustainable fungicides[7,8].

Plants use a variety of different mechanisms to resist fungal and oomycete infections [9]. Anti-microbial peptides (AMPs) are ubiquitous throughout the plant kingdom and play important roles in plant defense against fungal and oomycete pathogens. Their potent antifungal and anti-oomycete activity are important components of the plant innate immune system[8,10]. Defensins, in particular, are one of the largest families of AMPs expressed in plants. Because of their potent antifungal activity, diverse amino acid sequences and multi-target MoA, plant defensins have emerged as potential antifungal agents for agriculture[11-13]. They are 45-54 amino acids long, cysteine-rich, cationic peptides characterized by the presence of a cysteine-stabilized αβ motif. This motif consists of one α-helix and three antiparallel β-strands linked by three disulfide bonds. The fourth disulfide bond connects near the N- and C-termini and essentially cyclizes the peptide [14]. The cationic plant defensins exhibit potent broad-spectrum antifungal activity against fungal pathogens *in vitro* and *in planta*[13-16]. We set out to investigate if small, truncated peptides containing the active carboxy-terminal γ-core motif ($GXCX_{3-9}C$) of plant defensins exhibited potent fungicidal activity and were effective as spray-on fungicides for management of fungal diseases. We further investigated if the small defensin-derived peptides exhibited MoA different from those of the full-length parental peptide.

MtDef4 is an evolutionarily conserved 47-amino acid defensin from *Medicago truncatula* that exhibits broad-spectrum antifungal activity against fungal pathogens at low micromolar concentrations. Its MoA against a plant pathogen *Fusarium graminearum* involves plasma membrane permeabilization, binding to bioactive phosphatidic acid (PA), cell entry and presumed interaction with intracellular targets[17-19]. Like many other plant defensins, this peptide contains a well-characterized γ-core motif required for its antifungal activity[18,19]. A chemically synthesized C-terminal 16-amino acid sequence, designated GMA4C, containing this motif and a net charge of +6 inhibited the growth of the fungal pathogen *Fusarium graminearum in vitro* although its potency was four-fold lower than that of MtDef4[18]. This peptide also exhibited antifungal activity against crown rot fungal pathogens of alfalfa and, in addition, inhibited the growth of plant and human bacterial pathogens *in vitro*[20].

Herein, we explored the potential of the synthetic, MtDef4-derived, structurally less complex, 17-amino acid GMA4CG variants for development as fungicides. We characterized the antifungal activity of several GMA4CG variants generated via amino acid substitutions, C-terminal amidation, and disulfide cyclization that exhibited potent antifungal activity *in vitro* against an aggressive necrotrophic fungal pathogen *Botrytis cinerea*, causal agent of a gray mold disease in vegetables, fruits, and flowers. In sharp contrast to MtDef4, an interesting characteristic of GMA4CG variants was that they retained potent antifungal activity in media with elevated salt concentrations. Based on its superior *in vitro* and semi-*in planta* antifungal activity against *B. cinerea*, we focused on GMA4CG_V6 as the lead peptide for *in planta* antifungal activity and MoA studies. GMA4CG_V6 exhibited multi-faceted MoA and rapidly killed fungal cells. When sprayed on *Nicotiana benthamiana* and tomato plants, GMA4CG_V6 conferred strong preventative and curative antifungal activity against *B. cinerea* without detectable phytotoxicity.

Results

Design of short MtDef4-derived synthetic peptide variants

We based our work on the premise that a small MtDef4-derived peptide spanning the active γ-core motif could serve as a promising template for the design of peptide based fungicides. We further hypothesized that a small antifungal peptide would be more cell permeant and that with targeted amino acid substitutions of the γ-core motif, we could further enhance its antifungal potency. To test this hypothesis, we generated a truncated set of linear and cyclic variants of the 17-amino acid peptide spanning this motif (Gly30-Cys47) (**Fig. 1A**), designated GMA4CG, and tested them for antifungal activity against *B. cinerea.*

The substitution of each amino acid with all possible alternative amino acids in GMA4CG_WT is not practical. Thus, our strategy was to substitute cationic or hydrophobic residues in specific positions with the expectation that they would have significant influence on the antifungal activity of this peptide. MtDef4 is an evolutionarily conserved defensin in the plant kingdom and sequences of several homologs from various plants have been reported[19]. GMA4CG_V1 is a natural variant derived from the MtDef4 homolog (KHN09675.1) of *Glycine soja*. This natural variant has three amino acid differences (R5K, T15R and H16I) relative to the sequence of GMA4CG_WT. GMA4CG_V2 was generated to determine if substitution of one cationic acid with another had a notable impact on its antifungal activity. Thus, this variant carried a Lys5 to Arg substitution. We also designed peptide variants (GMA4CG_V3 to GMA4CG_V6) to test the influence of increased hydrophobicity on their antifungal activity. Thus, each of these variants has 29.4% hydrophobic amino acids as compared with 11.8% in GMA4CG_WT. GMA4CG_WT has four cysteine residues (Cys4, Cys11, Cys13 and Cys17) in its sequence, suggesting a potential to generate a pseudo-cyclic structure via disulfide bond formation between

Cys4 and Cys17. Cyclization has been reported previously to increase the antimicrobial activity and selectivity of AMPs [21,22]. Thus, we had cyclic GMA4CG_V3 and GMA4CG_V6 synthesized with a Cys4-Cys17 disulfide bond and replaced Cys11 and Cys13 with either an aliphatic Val (GMA4CG_V3) or an aromatic Trp (GMA4CG_V6) residue. Trp is more effective in interacting with the interfacial regions of lipid bilayers and it promotes antimicrobial activity of peptides[23-25]. All peptides were amidated at the C-terminus, a process known to increase the stability of peptides against proteolytic degradation, and therefore, also its biological activity[26].

GMA4CG_V4 and GMA4CG_V6 variants have potent antifungal activity

We assessed the antifungal activity of GMA4CG_WT and its six variants in SFM against *B. cinerea in vitro.* GMA4CG_WT inhibited the growth of these two fungi with the MIC value of 3 µM, four-fold higher than that of MtDef4 (**Fig. 1B**). Among all variants, only GMA4CG_V4 and GMA4CG_V6 displayed two-fold higher antifungal activity than GMA4CG_WT with the MIC value of 1.5 µM. These two peptides also inhibited the growth of *F. graminearum* with the MIC value of 1.5 µM (**Fig. 1B**).

To determine if GMA4CG_V6 had fungicidal or fungistatic activity, *B. cinerea* conidia were treated with 1.5 µM peptide for 1, 6, and 24 h. Following each treatment, the peptide was removed, and spore germination was examined under the microscope. Approximately, 85% of the conidia failed to germinate after 1 h of peptide challenge and nearly 100% of the conidia failed to germinate after 6 and 100% of the conidia failed to germinate after 24 h of treatment (**Fig S1A, B**). To assess further the toxicity of GMA4CG_V6, we stained peptide-treated conidial cells with propidium iodide, a cell death marker, and observed that nearly 80% of the conidia had stained red within 2 h of peptide treatment indicating fungicidal activity for this peptide (**Fig. S1C, D**).

At concentrations used GMA4CG variants, but not MtDef4, retained antifungal activity in presence of salts

Many naturally occurring AMPs, including plant defensins, are known to lose their antifungal activity in media containing elevated salt concentrations[27,28]. We determined the MIC values of GMA4CG_WT and its variants containing the R/KGFRRR motif in media containing 100 mM NaCl, 100 mM KCl or 2 mM $CaCl_2$ and compared them to that of MtDef4. At the highest concentration tested (6 µM), MtDef4 had no activity against *B. cinerea*. However, GMA4CG_WT and its variants retained their antifungal activity in salt supplemented media with varying degrees against this pathogen with GMA4CG_V4 and GMA4CG_V6 retaining the most potent antifungal activity (**Fig. 1B and Fig. S2A**). GMA4CG_V6 at 3 µM completely inhibited spore germination in presence of NaCl and $CaCl_2$ salts (**Fig. S2B**). GMA4CG_V6 was notably more effective than GMA4CG_V3 in presence of 100 mM KCl and 2 mM $CaCl_2$ (**Fig.1B and Fig. S2A**) indicating that Val to Trp substitution is important for salt-tolerant antifungal activity in these variants. Collectively, these data revealed that the MtDef4-derived GMA4CG_WT peptide and its variants with a net charge of +5 to +6 exhibited salt-tolerant antifungal activity. In contrast, the parental MtDef4 exhibited salt-sensitive antifungal activity at the concentrations used.

GMA4CG_WT and GMA4CG_V6 were predominantly random coils in structure

The three-dimensional (3D) structure of MtDef4 contained a γ-core motif composed of □-strands β2 and β3 connected by a positively charged RGFRRR loop[18]. The 3D structures of GMA4CG_WT and GMA4CG_V6 (our lead peptide) were modeled *de novo* using AlphaFold2[29]. The predicted structures shown in **Fig. 1C**, revealed that these peptides exist essentially in a random coil conformation with no classical elements of secondary structure. These models were

supported experimentally by the steady-state CD wavelength spectra for GMA4CG_WT and GMA4CG_V6 illustrated in **Fig. 1D.** Absent in both spectra are features characteristic of a peptide with α-helical (double minima at approximately 222 and 208 nm and an extrapolated maximum around 195 nm) or β-strand (single minimum at around 220 nm and an extrapolated maximum around 195 nm) secondary structure[30,31]. Instead, the dominant feature in both spectra was a minimum that extrapolates to wavelengths under 200 nm. Together, these features suggested that these peptides do not have α-helical or β-strand secondary structure content.

RRRW was a major determinant of the salt-tolerant antifungal activity of the linear GMA4CG_V6 without a disulfide bond

A series of linear alanine-substituted variants of our lead peptide GMA4CG_V6 (**Fig. S3A**) were tested to identify amino acids important for antifungal activity. The GMA4CG_V6_Ala3 variant carrying the substitution of RRRW with AAAA lost antifungal activity eight-fold, whereas all other variants lost antifungal activity four-fold (**Table 1, Fig S3B**). In SFM supplemented with 100 mM NaCl, no further loss in the antifungal activity of variants occurred except in GMA4CG_V6_Ala3, which lost antifungal activity another twofold (**Fig S3C**). These results indicated that RRRW motif is an important determinant of the antifungal activity of GMA4CG_V6 in media supplemented with salts.

GMA4CG_V4 and GMA4CG_V6 variants potently reduced gray mold disease symptoms semi-*in planta*

We compared the semi-*in planta* antifungal activity of GMA4CG_WT and its variants using detached leaves of *N. benthamiana* as described[28]. GMA4CG_WT and variants GMA4CG_V1

through GMA4CG_V5 were applied as drops of different concentrations on each leaf and freshly prepared conidial inoculum was immediately applied to each drop. Leaves were assessed for attenuation of gray mold symptoms by each peptide 48 h post-inoculation relative to no peptide controls by measuring lesion sizes and photosynthetic efficiency [as measured by Fv (variable fluorescence)/Fm (maximal fluorescence)]. Increasing concentration of each peptide significantly reduced lesion sizes (**Fig. 2A and B**). For all peptides, no lesions were formed at 6 µM. At 3 µM, only GMA4CG_V3 and GMA4CG_V4 were effective in suppressing lesion formation. At 1.5 µM, only GMA4CG_V4 completely suppressed disease symptoms. The photosynthetic efficiency data further supported GMA4CG_V4 as being more potent than the other five in reducing gray mold lesions **(Fig 2A).** We then compared the semi-*in planta* antifungal activity of GMA4CG_V4 and GMA4CG_V6. Both peptides completely suppressed disease symptoms at 1.5 and 3 µM under the applied conditions. However, at a lower concentration of 0.75 µM, GMA4CG_V6 was more effective in suppressing gray mold disease symptoms than GMA4CG_V4 **(Fig. 2C and D).**

GMA4CG_V6 enhanced permeability of the plasma membrane of *B. cinerea* spores and germlings

To determine if GMA4CG_V6 permeabilized the fungal plasma membrane, the spores and germlings of *B. cinerea* were treated with 1.5 µM GMA4CG_V6 for 30 min and SYTOX™ Green (SG) Nucleic Acid Stain was added. SG is a membrane-impermeant dye, which fluoresces when it binds to RNA and DNA and is a useful indicator of membrane permeability. SG uptake was observed in nearly all fungal spores and germlings challenged with this peptide, but not in controls without a peptide **(Fig. 3A)**. Thus, we concluded that GMA4CG_V6 MoA involved increased plasma membrane permeabilization.

Since antifungal activity of GMA4CG_V6 was cation-tolerant, we determined if membrane permeability still occurred in the presence of 100 mM KCl. In the absence of this salt, 95% of the conidia exposed to 1.5 µM GMA4CG_V6 for 1 h took up SG, indicating increased membrane permeability. No further time- or concentration dependent increase in membrane disruption was observed in the absence of this salt **(Fig. 3B).** By contrast, uptake of SG occurred in less than 10% conidia treated with 1.5 µM GMA4CG_V6 for 1 h in presence of 100 mM KCl. Even after 5 h, only ~17% of the conidia took up SG. Only at a high concentration of 6 µM, ~80% of conidia were permeabilized after 5 h **(Fig. 3B).** Thus, the membrane-permeabilization ability of GMA4CG_V6 was negatively impacted by the presence of cations; however, the peptide was still effective in permeabilizing the fungal plasma membrane at increased concentrations with longer exposure.

We also compared the ability of GMA4CG_V6 to permeabilize the plasma membrane using our SG assay in germlings with that of GMA4CG_WT and MtDef4 in absence and presence of 100 mM KCl. In absence of KCl, MtDef4 was more effective in permeabilizing the plasma membrane than GMA4CG_WT or GMA4CG_V6. However, in presence of this salt, MtDef4's ability to permeabilize the plasma membrane was completely lost. In contrast, GMA4CG_WT and GMA4CG_V6 retained their ability to permeabilize the plasma membrane **(Fig. 3C)**.

GMA4CG_V6 was internalized into the vacuole and cytoplasm of *B. cinerea* in a time and concentration dependent manner

The tetramethyl rhodamine (TMR)-labeled GMA4CG_V6 was imaged using time-lapse confocal microscopy to gain insight into the temporal nature of peptide internalization in germlings of *B. cinerea*. At MIC of 1.5 µM, the labeled peptide first bound to the cell surface within the first 3

min and started translocating into vacuoles from multiple entry foci by 19 min **(Fig. 4A)**. At this time point, brightfield images of germlings showed abnormal morphology with their vacuole boundaries becoming visible. At 27 min, the vacuoles began to expand by coalescence of small vacuoles and the peptide localized into cytoplasm. Shortly after the peptide appeared in the cytoplasm the vacuoles appeared to lyse with the peptide rapidly dispersing throughout the germling cytoplasm and inducing cell death **(Fig. 4A)**.

At a sub-lethal concentration of 0.5 µM, the labeled peptide bound to the surface of germlings and formed presumptive endosomal bodies in the cytoplasm. No further progression of the peptide in the germling cells occurred during the 1 h challenge **(Fig. S4A)**. At high concentration (20 µM), TMR-labeled GMA4CG_V6 was internalized by germlings as early as 4 min. Without entering endosomes or vacuoles, the peptide rapidly accumulated in the germling cytoplasm and within 13 min was completely dispersed throughout the cell's interior **(Fig. S4B)**. This suggests that at high concentrations, GMA4CG_V6 may bypass intermediate endosome or vacuole localization and accumulate directly in the cytoplasm. This may be a critical step in inducing cell death at elevated GMA4CG_V6 concentrations.

The subcellular localization of TMR-GMA4CG_V6 was determined using two dyes which specifically stain membranes (FM4-64) and vacuole lumen (CMAC). Within 30 min of peptide challenge, TMR-GMA4CG_V6 co-localized with CMAC in the vacuole, and with FM4-64 at the plasma membrane and entry foci in germlings **(Fig. 4B)**. Based on the region of interest (ROI01) in **Fig. 4B**, the fluorescence intensity curve clearly showed that the peak signal of TMR-GMA4CG_V6 overlapped with the signal of FM4-64 in membrane and CMAC in vacuole **(Fig. 4C)**. After 60 min, the labeled peptide remained in the vacuole but showed extensive co-localization with the cytoplasm **(Fig. 4D, E)**. To determine whether GMA4CG_V6 bound to the

cell wall of *B. cinerea*, a cell wall specific dye Calcofluor White (CFW) was used to incubate with TMR-GMA4CG_V6 treated *B. cinerea* germlings. As illustrated in **Figure S5A and B**, CFW overlapped with TMR fluorescent signal in images captured by confocal microscopy. Considering the thickness of cell wall and the limitation of the resolution of the confocal microscopy, super-resolution microscopy was used to further test the co-localization of TMR-GMA4CG_V6 with cell wall. It was interesting that the fluorescent signal of CFW and TMR seemed perfectly overlapping in the image **(Fig. S5C)**, but the intensity curve of each signal showed a bit shifting based on the ROI **(Fig. S5D)** as shown by arrows. The super-resolution microscopy with HILO illumination mode was used to further understand the co-localization of TMR-GMA4CG_V6 with CFW. Near to the cell surface area, TMR-GMA4CG_V6 showed declining signal compared with the CFW signal **(Fig. S5E)**, indicating that TMR-GMA4CG_V6 and CFW did not overlap perfectly over the entire cell wall region.

To further study the binding affinity of GMA4CG_V6 to specific subcellular components in *B. cinerea* germlings, a series of Fluorescence Recovery After Photobleaching (FRAP) experiments were performed **(Fig. S6A-C)**. We specifically studied the mobility of TMR-GMA4CG_V6 to subcellular components including germling cell walls, vacuoles, and cytoplasm. In our previous study, a significant difference in the mobility of the antifungal peptide NCR044 to germling and conidial cell walls was observed[32], thus, we performed FRAP experiments with conidial cell walls as well. According to the normalized fluorescence recovery curve, TMR-GMA4CG_V6 recovery in the germling cytoplasm had the greatest overall mobility among all four targeted components and the mobility in vacuoles was relatively low **(Fig. S6A)**. Immobile fraction and half time of fluorescence recovery data were also collected as summarized in **Fig. S6B, C**. GMA4CG_V6 in germling vacuoles showed a significantly higher ($p < 0.0001$) immobile

fraction (82.6± 3.2%) than other subcellular components and the recovery time was much shorter (Tau= 19.27 sec, R^2= 0.8496). In cell walls of germlings and conidia, no significant difference was observed in the immobile fraction (52.5 ± 4.2% and 51.0 ± 4.9%, respectively, p> 0.05) or in the half recovery time (37.4 sec, R^2= 0.9133 and 38.4 sec, R^2= 0.9257). The immobile fraction of the peptide was lower (p= 0.0031) in germling cytoplasm (35.2 ± 4.3%) as compared to that in germling cell wall and vacuole but showed no significant difference with that of the conidial cell wall. The Tau value of peptides in germling cytoplasm was the highest among the four selected subcellular components (Tau= 40.68 and R^2= 0.9636). Collectively, the FRAP analysis indicates that the mobility of the peptide in the cell wall and cytoplasm is similar but not in the vacuole. The low mobility in vacuole is likely due to the fact that membrane transport to the vacuole is not a continuum like other comportments and multistep mobility in the vacuole itself would be very high as the cure and Tau values show.

Because of the difference in the cation tolerant antifungal activity of MtDef4 and GMA4CG peptides, we examined the binding of MtDef4, GMA4CG_WT and GMA4CG_V6 to the conidia of *B. cinerea* in presence of 100 mM KCl. The fluorescently labeled MtDef4 bound to the cell surface in absence of this salt. However, this binding was significantly reduced in presence of this salt (p= 0.001). In contrast, binding of GMA4CG_WT and GMA4CG_V6 to the cell surface was not affected by salt (p> 0.05) **(Fig. 4F, G)**.

Next, we examined if internalization of GMA4CG_V6 into *B. cinerea* germlings was energy-dependent and if actin played a role. Germlings were challenged with GMA4CG_V6 in the presence of Latranculin A (LatA), an inhibitor of actin polymerization, and sodium azide (NaN_3), an inhibitor of mitochondrial respiration. Although these inhibitors did not block binding of this peptide to the cell surface, they inhibited internalization of the peptide into the vacuoles of

germling cells **(Fig. S7A)**. It is worth noting that while no peptide was observed entering into the vacuoles, fluorescent signal was visible in the cytoplasm after extended exposure. In contrast, Brefeldin A, an inhibitor of the ER-to-Golgi secretory pathway, did not inhibit the uptake and entry of GMA4CG_V6 into vacuoles with the staining pattern similar to that observed in the "No inhibitor" control. Interestingly, prevention of the vacuolar localization of GMA4CG_V6 by LatA or NaN_3 did not reduce the spore germination inhibitory activity of GMA4CG_V6 since conidia treated with peptide or with peptide plus LatA or NaN_3 showed no statistically significant differences ($p>0.05$) in germination **(Fig. S7B)**. Overall, these results indicated that actin polymerization played a role in GMA4CG_V6 internalization and vacuolar localization and that this process was energy-dependent at the concentrations tested. Blocking internalization of the peptide into vacuoles did not influence the MIC of GMA4CG_V6.

GMA4CG_WT and GMA4CG_V6 bind to multiple phosphoinositides

MtDef4 binds to phosphatidic acid (PA) in fungal membranes as part of its MoA[18]. Therefore, we tested if MtDef4-derived GMA4CG_V6 also binds to PA. A protein-lipid overlay assay was performed with various biologically active phospholipids immobilized on a lipid strip (Echelon Bioscience, UT). GMA4CG_V6 bound to several phosphoinositides including phosphatidylinstol (PI) mono- and bisphosphates, PA and phosphatidylserine, but with higher affinity for PI4P and PI5P than for PA **(Fig. S8)**. GMA4CG_WT also bound to the same phospholipids as GMA4CG_V6. His_6 alone used as a C-terminal tag for each peptide did not bind to any phospholipids. These results indicate that GMA4CG_V6 is more promiscuous in its binding to plasma membrane resident phospholipids than MtDef4[18].

Spray-applied GMA4CG_V6 provided preventative and curative antifungal activity against gray mold disease

We tested the potential of GMA4CG_WT and GMA4CG_V6 to provide preventative protection from gray mold disease by spraying four-week-old *N. benthamiana* plants with each peptide at concentrations of 12 and 24 µM followed 2 h later with the spray-inoculum of *B. cinerea* conidia. Each peptide spray-applied at 12 or 24 µM significantly reduced gray mold disease symptoms compared with control plants inoculated with pathogen only **(Fig. 5A and Fig. S9A)**. Both peptides significantly prevented the spread of gray mold on *N. benthamiana* plants **(Fig. 5A & 5B)**. Notably, plants sprayed with GMA4CG_V6 and subsequently inoculated with the pathogen looked as symptom free as non-inoculated mock (water)-sprayed plants. This data clearly demonstrated higher potency of GMA4CG_V6 than GMA4CG_WT in reducing gray mold disease in *N. benthamiana* plants in a preventative manner. In addition, GMA4CG_V6 is significantly ($P < 0.0001$) more effective in limiting disease severity when applied at 24 µM than at 12 µM ($P = 0.0278$) **(Fig. S9A & B)**.

We also tested GMA4CG_WT and GMA4CG_V6 for their ability to provide curative protection from this disease at three different time points following fungal infection. *N. benthamiana* plants were pre-inoculated with freshly prepared *B. cinerea* spores for 2, 15 and 30 h after which each peptide at 12 µM was sprayed onto the plants. *B. cinerea* spores germinate after 12 h [33], and thus, fungal infection of the leaf surface has already occurred at 15 and 30 hpi. Disease symptoms were rated at 72 hpi. Both peptides provided significant curative ($p = 0.0019$) protection from gray mold **(Fig. 5C and Fig. S9C)**. However, GMA4CG_V6 conferred significantly greater ($p < 0.0001$) curative antifungal activity than GMA4CG_WT sprayed on plants pre-inoculated for 15 h **(Fig. 5D)**. The reduced disease severity in GMA4CG_V6 sprayed plants further confirmed

greater efficacy of this peptide **(Fig. S9C)**. In plants pre-inoculated for 2 h or 30 h, both peptides provided robust control of disease symptoms with similar efficacy **(Fig. 5D & S9D)**. Furthermore, our data showed the potential of GMA4CG_V6 in reducing the spread of disease symptoms **(Fig. S9D)**.

Next, we tested the curative antifungal activity of GMA4CG_WT and GMA4CG_V6 on tomato (cv. Mountain Spring) plants pre-inoculated for 12 h and subsequently sprayed with each peptide at a concentration of 6, 12 and 24 µM. Both peptides conferred curative antifungal activity at all three concentrations **(Fig. 6A)**. At concentrations of 12 and 24 µM, no significant difference was observed between the two peptides in their ability to reduce disease symptoms. Both peptides provided robust curative protection with pathogen-challenged plants appearing similar to water-sprayed non-inoculated mock plants. However, at a concentration of 6 µM, GMA4CG_V6 conferred significantly greater ($p < 0.0001$) curative antifungal activity than GMA4CG_WT **(Fig. 6B)**.

Further, visual rating of disease severity clearly revealed superiority of GMA4CG_V6 in controlling gray mold disease in tomato plants **(Fig. S10A & B)**. The CW staining of the tomato leaves from control plants infected with pathogen alone and from infected plants sprayed with GMA4CG_V6 confirmed strong inhibition of fungal growth caused by this peptide **(Fig. 6C)**.

GMA4CG_V6 binds strongly to the tomato leaf surface and is not internalized into plant cells

To determine the fate of GMA4CG_WT and GMA4CG_V6 on leaf surfaces, fluorescently labeled peptide was applied onto detached tomato leaves and the uptake of each peptide by the plant cells was followed using confocal microscopy. In leaves with no applied peptide, only auto-fluorescent

signal from the plant cells was observed **(Fig. S11A)**. Both GMA4CG_WT and GMA4CG_V6 bound to the exterior of plant cell walls, but no internalization into plant cells was detected **(Fig. S11B)**. After washing the leaves under water, the fluorescence intensity of GMA4CG_WT was significantly reduced ($p < 0.0001$) but that of GMA4CG_V6 was only slightly reduced ($p = 0.1146$) **(Fig. S11C)**. This result suggests that GMA4CG_V6 adheres to the tomato leaf surface more tightly than GMA4CG_WT making it more rainfast.

GMA4CG_V6 has no effect on *N. benthamiana* seed germination and seedling growth

We assessed the phytotoxicity of GMA4CG_V6 by testing its effect on the germination of *N. benthamiana* seeds in presence of the peptide at concentrations ranging from 12 to 96 µM and observed that the peptide did not prevent seed germination **(Fig. S12A, B)** albeit, seedlings appeared light green in color and root lengths shorter at higher concentrations (48 and 96 µM) of GMA4CG_V6. We also sprayed one-week-old *N. benthamiana* seedlings with 24 µM peptide or water alone. One-week post peptide application, we observed no difference in the growth of the peptide-sprayed seedlings and the water-sprayed seedlings nor any signs of stress in CropReporter images **(Fig. S12C, D)**.

Discussion

Modern agriculture relies heavily upon systemic single-site fungicides with preventative and curative antifungal properties. However, rapid evolution of fungal resistance to fungicides poses a major threat to crop protection and food security worldwide. New environmentally friendly antifungal compounds with multifaceted MoAs are needed to mitigate resistance development.

Here, inspired by the broad-spectrum antifungal activity, structure, and multi-faceted MoA of the plant defensin MtDef4, we explored the potential of a short 17-residue peptide for development as a peptide based fungicide.

We designed and synthesized six 17-amino acid GMA4CG variants spanning the active γ-core motif of a plant defensin MtDef4[17-19]. We made several modifications of the GMA4CG peptide that maintained or enhanced its antifungal activity against an economically important fungal pathogen *B. cinerea*. Although we could not perform complete analysis of all amino acid substitutions, our selected changes revealed the importance of cationic and hydrophobic residues for antifungal activity of this peptide. Amino acids we chose to replace, were guided partly by the corresponding amino acid sequences of the homologs of MtDef4 from other plants. In addition, replacement of the internal Cys_{11} and Cys_{13} residues to the aromatic hydrophobic amino acid Trp enhanced antifungal activity. The importance of Trp at these positions was revealed by our observation that an aliphatic hydrophobic residue Val at these positions was less effective. It is likely that interactions of the two Trp residues with the Arg residues present in the GMA4CG_V6 primary amino acid sequence contribute significantly to peptide stability[34]. Further, Trp is known to insert into membranes containing anionic phospholipid head groups with high efficiency, thus contributing to the increased fungal membrane permeability by this designed peptide[35]. We synthesized GMA4CG_V6 as a cyclic peptide with a disulfide bond connecting Cys4 and Cys17 with the notion that it would be more stable, more fungal cell permeable, more readily internalized into fungal cells, and confer higher antifungal activity than its linear counterpart. Cyclic peptides are touted as promising antimicrobial molecules since they are stable to proteolytic degradation, have high affinity and selectivity for targets, and better cell membrane permeability[36].

Structural studies using AlphaFold2 predicted GMA4CG_WT and GMA4CG_V6 each had random coil/unordered structures. These *in silico* AlphaFold2 predicted structures were corroborated experimentally by steady-state wavelength CD spectra showing the absence of any significant α-helical or β-strand secondary structure content[30,31]. The notable difference between the CD spectra of the two peptides was an additional minor minimum at ~230 nm for GMA4CG_WT and a minor maximum at ~ 230 nm for GMA4CG_V6. In combination with the major sub-220 nm minimum, the former feature is characteristic of a random coil/unordered structure and the latter feature characteristic of a polyproline II structure suggesting the multiple amino acid substitutions may induce a transition of some random coil to polyproline II structure in GMA4CG_V6[37].

Antifungal activity of several cationic plant defensins is abrogated in well-defined synthetic fungal growth medium containing elevated levels of Na^+ or Ca^{2+} [27,28,38,39]. At the highest concentration of 6 µM tested, MtDef4 exhibited no antifungal activity against *B. cinerea* in medium containing elevated levels of Na^+, K^+, or Ca^+. The presence of cations likely weakens the electrostatic interactions between this cationic plant defensin and negatively charged fungal membranes. Surprisingly, all six truncated peptide variants derived from MtDef4 exhibited antifungal activity against *B. cinerea* in fungal growth medium containing elevated levels of Na^+, K^+ or Ca^{++}. Among the six variants, GMA4CG_V6 was the most potent antifungal agent. The molecular basis for cation-tolerant antifungal activity of these peptides is unclear currently. However, it is clear that RRRW motif plays an important role in conferring cation-tolerant antifungal activity.

The structure and MoA of GMA4CG_V6 are unlike those of any fungicide currently on the market. The preventative and curative plant protection properties of GMA4CG_V6 is likely

due to its ability to kill fungal pathogens rapidly. It does not have a discrete intracellular molecular target, but instead interferes with multiple cellular processes **(Fig. 7)**. A major characteristic of antifungal peptides is their ability to permeabilize the plasma membrane of fungal pathogens. GMA4CG_V6 quickly binds to the cell surface of fungal spores and germlings and subsequently disrupts the plasma membrane of these cells near the entry points. GMA4CG_V6 enters the interior of the fungal cell in an energy-dependent manner and actin polymerization plays a role in this process. The co-localization of GMA4CG_V6 with the vacuolar dye CMAC revealed that this peptide, at MIC values, localizes to vacuoles in germlings of *B. cinerea*. However, it remains to be determined if vacuole localization is required for the antifungal activity of this peptide. It is of interest to note that a small rationally designed antifungal hexapeptide PAF26 with the sequence Ac-RKKWFW-NH_2 also localizes to vacuoles in the model fungus *Neurospora crassa*[40]. Like PAF26, GMA4CG_V6 at MIC enters vacuoles and causes their expansion and lysis. It subsequently accumulates in the cytoplasm. At elevated concentration, GMA4CG_V6 appeared to accumulate rapidly in the cytoplasm. MtDef4 binds to the bioactive phospholipid PA as part of its MoA[17,18]. In contrast, GMA4CG_V6 derived from this defensin binds to multiple bioactive phospholipids including PA. It preferentially binds to the phosphoinositides PIPs in the phospholipid-protein overlay assay. Further studies are needed to understand the role promiscuous interactions with multiple phospholipids play in the multi-faceted MoAs of GMA4CG_V6.

Current crop protection research is guided by a strong demand for sustainable fungicides that are efficacious, less prone to resistance development, environmentally friendly, and nonphytotoxic. In semi-*in planta* antifungal assays using detached *N. benthamiana* leaves, all six GMA4CG analogs significantly reduced gray mold disease lesions caused by *B. cinerea* infection with GMA4CG_V6 proving most effective. Under the conditions employed, spray application of

GMA4CG_V6 conferred strong preventative and curative antifungal activity against this disease in young *N. benthamiana* and curative antifungal activity in tomato. These fungicidal effects were observed readily even though the dose, application frequency, and distribution formulation have yet to be optimized. In our studies, GMA4CG_V6 was more effective than GMA4CG_WT in reducing disease symptoms suggesting that the amino acid substitutions introduced in GMA4CG_V6 are important for its *in vitro* as well as *in planta* antifungal activity. Although defensin-derived peptides offer the benefits of small size, structural simplicity and efficiency of peptide modifications, their commercial use as peptide fungicides will require new innovations in peptide production at scale to be economical. In addition, efficacy of these peptides for fungal disease control will need to be assessed in large-scale field trials and their stability to proteolytic degradation and potential phytotoxicity will also need to be evaluated in field studies.

Recent studies have shown the promise of antifungal peptides as topical fungicides. A fusion of the animal AMP dermaseptin and thanatin inhibits the germination of the spores of the obligate biotrophic fungal pathogen *Phakopsora pachyrhizi* and reduces the symptoms of Asian rust when spray-applied to soybean leaves[41]. Spray-application of the antifungal peptide NCR044 from *M. truncatula* on tomato and *N. benthamiana* plants provided protection from the gray mold disease [32]. The present study showed that a designed defensin-derived peptide with multi-faceted MoA exhibited excellent preventative and curative antifungal activity against the gray mold disease of plants. Hundreds of sequences divergent antifungal plant defensins in the AMP database can now be exploited as templates for design and development of small peptide-based fungicides with diverse MoA for future use in agriculture[12,42].

Methods

Fungal cultures and spore suspensions

The fungal strains *Botrytis cinerea* T-4 and *Fusarium graminearum* PH-1 were each cultured in their respective normal growth medium shown in **Table S1**. Fungal spores were harvested by flooding the fungal growth plates with sterile water. The spore suspension was filtered through two layers of Miracloth, centrifuged at 13,600 rpm for 1 min, washed, and re-suspended in low-salt Synthetic Fungal Medium (SFM)[43]. The spore suspension of each fungal pathogen was adjusted to the desired spore density of ~10^5 spores/mL using a hemocytometer.

Peptide synthesis and purification

The peptides GMA4CG_WT and GMA4CG_V1-V6 were chemically synthesized with an initial purity of ~80-85% from multiple commercial vendors and further purified using a C-18 reverse phase HPLC as described[32]. The HPLC fractions containing the peptide were lyophilized and re-suspended in the nuclease-free water. Peptide concentrations were determined using both the BCA assay kit (Thermo-Fisher Scientific, USA) according to the manufacturer's protocol and NanoDrop 2000c Spectrophotometer (Thermo-Fisher Scientific, USA) (for the peptides having tryptophan).

Antifungal activity assays

The minimal inhibitory concentration (MIC) of each peptide was determined using the resazurin cell viability assay[28,44]. Briefly, this involved incubation of the pathogen/peptide mixture for 48 h, adding 0.01% (w/v) resazurin solution to each well, and re-incubating overnight. A change in color of the resazurin dye from blue to pink or colorless indicated the presence of live fungal cells. MIC was determined as the minimal concentration of peptide at which no change in color was observed.

The MIC value of each peptide was also determined in SFM supplemented with 100 mM NaCl, 100 mM KCl, or 2 mM $CaCl_2$.

Circular dichroism spectroscopy

A steady-state wavelength circular dichroism spectrum was collected for GMA4CG_WT and GMA4CG_V6 (~0.05 mM peptide, 20 mM sodium acetate, pH 5.6) on a calibrated Aviv Model 410 spectropolarimeter (Lakewood, NJ). Using a quartz cell of 0.1 cm path length and a temperature of 20 °C, the data was recorded in 0.5 nm increments between 200 and 260 nm with a bandwidth of 1.0 nm and a time constant of 1.0 s. The reported steady-state wavelength spectrum was the result of averaging two consecutive scans, subtracting a blank spectrum, and automatic line smoothing using Aviv software.

Membrane permeabilization assay using SYTOX™ Green (SG) uptake

The fluorescent dye SG (Thermo-Fisher Scientific) was used to identify GMA4CG_V6-induced membrane permeabilization of *B. cinerea* conidia and germlings as described previously[28]. After exposure to 1.5 µM GMA4CG_V6 for 30 min, *B. cinerea* spores and germlings were imaged using fluorescence microscopy on a Leica SP8-X confocal microscope with an excitation and emission wavelength of 488 and 508-544 nm, respectively.

The GMA4CG_V6 induced membrane permeabilization of conidia was also assessed quantitatively in the absence and presence of 100 mM KCl. Fresh conidia at a concentration of 1×10^5/mL were incubated with GMA4CG_V6 at 1×, 2×, and 4× MIC for 1 h in the absence and presence of 100 mM KCl for 1 h and 5 h, respectively. Samples were deposited into glass-bottom petri dishes and imaged by confocal microscopy at an excitation wavelength of 488 nm and an emission wavelength ranging from 508 to 544 nm in the presence of 1 µM SG added 15 min prior imaging. Fresh conidia incubated with SG alone were used as negative controls. A Leica SP8-X

confocal microscope was used for all confocal imaging and Leica LASX (version 3.1.5.) software was used to process the images. The percentage of conidia showing membrane permeabilization was determined by counting the number of cells showing fluorescent signal relative to the total number of cells counted.

The effect of MtDef4, GMA4CG_WT and GMA4CG_V6 on membrane integrity of *B. cinerea* germlings was determined using SG (final concentration: 1 µM) uptake quantification assay in presence and absence of 100 mM KCl[32]. In brief, membrane permeabilization in *B. cinerea* germlings treated with different concentrations (0.187, 0.375, 0.75, 1.5 and 3 µM) of MtDef4, GMA4CG_WT and GMA4CG_V6 was measured every 1 h for 5 h in presence and absence of 100 mM KCl. SG uptake was quantified by measuring the fluorescence in a SpectraMax® M3 spectrophotometer (exc: 488; cutoff: 515; emi: 530 nm).

Internalization and subcellular localization of GMA4CG_V6 in *B. cinerea* germlings

Time-lapse confocal laser scanning microscopy was used to monitor uptake and subcellular localization of fluorescently labeled peptide as described previously[32]. Crude TMR fluorophore labeled GMA4CG_V6 (TMR-GMA4CG_V6) was custom synthesized (Agentide Co, Piscataway, NJ) and purified by HPLC. *B. cinerea* germlings were generated by incubating conidia overnight in SFM medium. They were challenged with TMR-GMA4CG_V6 at concentrations of 0.5, 1.5, or 20 µM, and imaged by time-lapse confocal microscopy. The excitation and emission wavelengths for imaging TMR-GMA4CG_V6 were 562 nm and 580 to 680 nm, respectively.

The sub-localization of GMA4CG_V6 was determined by visualizing its co-localization with the vacuole-specific dye CMAC and the cell membrane specific dye FM4-64. The excitation and emission wavelengths for CMAC are 353 nm, 405 to 480 nm, respectively, and for FM4-64 are 562 nm and 680 to 800 nm, respectively. Co-localization analysis of TMR-GMA4CG_V6 and

CMAC/ FM4-64 was performed using Leica LAS-X software. The threshold for each channel was 50% and the pixels out of this range were considered uncorrelated. The threshold for background was set as 20%. Images were captured at 30 min and 60 min after incubation with peptide. Pearson's correlation and co-localization rate were collected to indicate whether the two fluorescent signals were correlated or not based on the region of interest (ROI) area.

Quantification of cell surface binding intensity

The spores of *B. cinerea* were treated with 1.5 µM DyLight550-labeled MtDef4, TMR-GMA4CG_WT and TMR-GMA4CG_V6 for 20 min. Spores of each treatment were imaged using a C-Apochromat 63X water immersion objective lens in apotome mode with ZEISS Elyra7 super-resolution microscope at excitation and emission wavelengths of 561 nm and 590 nm. Images were processed using the SIM^2 module and 2.5D processing in ZEN Black 3.0 SR FP2 software. For each captured cell, the cell surface binding intensity was quantified by free hand drawing a line intensity profile along the cell surface. The fluorescence intensity of each cell wall periphery was normalized by its perimeter length as described in[45]. The lower threshold was set to 7000 to subtract the signal in cytoplasm.

Semi-*in planta* antifungal activity assays

The semi-*in planta* antifungal activity of each peptide against *B. cinerea* was determined using *N. benthamiana* Nb1 detached leaves as described previously[28]. Each peptide was tested at concentrations ranging from 0.75, 1.5, 3, and 6 µM. Following incubation of each peptide/fungal spore mixture at room temperature for 48 h, leaves were photographed in white light. High-resolution fluorescence images were also taken using CropReporter (PhenoVation, Wageningen, Netherlands). These images depicted the calculated F_V/F_M (maximum quantum yield of photosystem II) values of diseased area affected by *B. cinerea* infection. Colors in the images show

five different classes ranging from class I to class V (0.000 to 0.700) depicting varying degrees of tissue damage. On one end of the scale, green color represents class V (0.600 to ≥0.700) high photosynthesis efficiency. On the other end of the scale, red color represents class I (0.000 to 0.160) low photosynthesis efficiency.

***In planta* antifungal activity assays**

To test preventative and curative antifungal activity of the peptides against *B. cinerea*, four-week-old *N. benthamiana* Nb1 plants grown under controlled growth conditions were used. For preventative activity, GMA4CG_WT and GMA4CG_V6 at 12 or 24 µM concentration were sprayed (2 mL/plant) on experimental plants. Control plants were sprayed with 2 mL of water/plant. The peptide solution or water was allowed to dry out on the surface of the leaves. *B. cinerea* spores (~$8x10^4$) suspended in 0.5 x SFM were sprayed on the experimental and control tomato plants (1 mL/plant), transferred to a Ziploc plastic box under high humidity, and disease symptoms recorded after 48 h. Photographs were taken at 72 h post-inoculation using both white light and CropReporter (PhenoVation, Wageningen, Netherlands). Quantification of symptoms was made by determining maximum quantum yield of PSII (Fv/Fm) as described above for semi-*in planta* assays.

For the curative antifungal activity tests, *N. benthamiana* Nb1 plants of similar age were first sprayed with *B. cinerea* spores (~$8x10^4$) suspended in 0.5 X SFM (1 mL/plant). After 2, 15, and 30 h of pathogen challenge, 2 mL of GMA4CG_WT or GMA4CG_V6 was sprayed on the plants at a concentration of 12 µM. Control plants were each sprayed with 2 mL of water. Disease symptoms were observed after 48 h of pathogen challenge. Plants were photographed at 72 h post infection in white light and quantification was done as described above. The curative antifungal activity of GMA4CG_WT and GMA4CG_V6 at concentration of 6, 12 and 24 µM was tested on

3-week-old tomato (*Solanum lycopersicum* L. cv. Mountain Spring) plants pre-inoculated with *B. cinerea* for 12 h. The severity of disease symptoms was rated using the scoring method for each inoculated plant as follows: 0, no symptoms; 1=1-25%, 2=26-50%, 3=51-75% and 4=76-100% of leaf surface infected.

Visualization of fungal growth on tomato leaf surface

Fresh *B. cinerea* conidia were collected and sprayed on 2-week-old tomato leaves surface and allowed to germinate for 12 h. After that, GMA4CG_V6 at 6 µM was applied on the same leaves and incubated in a container under high humidity. Leaves applied with spores and sterile water were set as negative controls. After 48 hours, leaves were fixed in 4% paraformaldehyde, stained with CFW for 30 min, and images were captured by Zeiss Axio Zoom.V16 microscope with PlanNeoFluar Z 1.0x objective under tile mode. The excitation wavelength was 335-383 nm, and the emission wavelength was 420-470 nm. Images were visualized and processed using Zeiss Zen Black.

References

1. Fones, H.N. *et al.* Threats to global food security from emerging fungal and oomycete crop pathogens. *Nature Food* **1**, 332-342 (2020).
2. Fisher, M.C. *et al.* Emerging fungal threats to animal, plant and ecosystem health. *Nature* **484**, 186-94 (2012).
3. Savary, S. *et al.* The global burden of pathogens and pests on major food crops. *Nature Ecology & Evolution* **3**, 430-439 (2019).

4. Fisher, M.C., Hawkins, N.J., Sanglard, D. & Gurr, S.J. Worldwide emergence of resistance to antifungal drugs challenges human health and food security. *Science* **360**, 739-742 (2018).

5. Oliver, R.P. & Hewitt, H.G. Fungicides in crop protection. in *Fungicides in Crop Protection.* 123-150 (Second edition, CAB International, Oxfordshire, Boston., 2014).

6. Hawkins, N. J., & Fraaije, B. A. Contrasting levels of genetic predictability in the evolution of resistance to major classes of fungicides. *Mol. Ecol*. **30**, 5318-5327, doi:10.1111/mec.15877 (2021).

7. Lobo, F. & Boto, A. Host defense peptides as new generation phytosanitaries: low toxicity and low induction of antimicrobial resistance. *Agronomy* **12**, 1614. (2022).

8. van der Weerden, N.L., Bleackley, M.R. & Anderson, M.A. Properties and mechanisms of action of naturally occurring antifungal peptides. *Cell Mol Life Sci* **70**, 3545-70 (2013).

9. van Esse, H.P., Reuber, T.L. & van der Does, D. Genetic modification to improve disease resistance in crops. *New Phytol* **225**, 70-86 (2020).

10. Goyal, R.K. & Mattoo, A.K. Multitasking antimicrobial peptides in plant development and host defense against biotic/abiotic stress. *Plant Sci* **228**, 135-49 (2014).

11. Cools, T.L., Struyfs, C., Cammue, B.P. & Thevissen, K. Antifungal plant defensins: increased insight in their mode of action as a basis for their use to combat fungal infections. *Future Microbiol* **12**, 441-454 (2017).

12. Parisi, K. *et al.* The evolution, function and mechanisms of action for plant defensins. *Semin Cell Dev Biol* **88**, 107-118 (2019).

13. Leannec-Rialland, V. *et al.* Use of defensins to develop eco-friendly alternatives to synthetic fungicides to control phytopathogenic fungi and their mycotoxins. *J Fungi* **8, doi:** 10.3390/jof8030229 (2022).

14. Kovaleva, V., Bukhteeva, I., Kit, O.Y. & Nesmelova, I.V. Plant defensins from a structural perspective. *Int J Mol Sci* **21,** doi: 10.3390/ijms 21155307 (2020)

15. Kaur, J., Sagaram, U.S. & Shah, D.M. Can plant defensins be sused to engineer durable commercially useful resistance in crop plants? *Fungal Biol Rev* **25**, 128-135 (2011).

16. Lacerda, A.F., Vasconcelos, E.A., Pelegrini, P.B. & Grossi de Sa, M.F. Antifungal defensins and their role in plant defense. *Front Microbiol* **5**, 116 (2014).

17. El-Mounadi, K., Islam, K.T., Hernandez-Ortiz, P., Read, N.D. & Shah, D.M. Antifungal mechanisms of a plant defensin MtDef4 are not conserved between the ascomycete fungi *Neurospora crassa* and *Fusarium graminearum*. *Mol Microbiol* **100**, 542-59 (2016).

18. Sagaram, U. *et al.* Structural and functional studies of a phosphatidic-acid binding antifungal plant defensin MtDef4: Identification of an RGFRRR motif governing fungal cell entry. *PLoS One* **8**, *e82485* (2013).

19. Sagaram, U. *et al*. Structure-activity determinants in antifungal plant defensins MsDef1 and MtDef4 with different modes of action against *Fusarium graminearum*. *PLoS One* **6**, e18550 (2011).

20. Sathoff, A.E., et al. Plant defensin peptides have antifungal and antibacterial activity against human and plant pathogens. *Phytopathol* **109**, 402-408 (2019).

21. Dathe, M., Nikolenko, H., Klose, J. & Bienert, M. Cyclization increases the antimicrobial activity and selectivity of arginine- and tryptophan-containing hexapeptides. *Biochemistry* **43**, 9140-50 (2004).

22. Tucker, A.T. *et al.* Discovery of next-generation antimicrobials through bacterial self-screening of surface-displayed peptide libraries. *Cell* **172**, 618-628 e13 (2018).

23. Deslouches, B. *et al. De novo* generation of cationic antimicrobial peptides: influence of length and tryptophan substitution on antimicrobial activity. *Antimicrob Agents Chemother* **49**, 316-22 (2005).

24. Chan, D.I., Prenner, E.J. & Vogel, H.J. Tryptophan- and arginine-rich antimicrobial peptides: structures and mechanisms of action. *Biochim Biophys Acta* **1758**, 1184-202 (2006).

25. Killian, J.A. & von Heijne, G. How proteins adapt to a membrane-water interface. *Trends Biochem Sci* **25**, 429-34 (2000).

26. Lu, J. *et al.* D- and unnatural amino acid substituted antimicrobial peptides with improved proteolytic resistance and their proteolytic degradation characteristics. *Front Microbiol* **11**, 563030 (2020).

27. Kerenga, B.K. *et al.* Salt-tolerant antifungal and antibacterial activities of the corn defensin ZmD32. *Front in Microbiol* **10,** 795 (2019).

28. Li, H., Velivelli, S.L. & Shah, D.M. Antifungal potency and modes of action of a novel olive tree defensin against closely related ascomycete fungal pathogens. *Mol Plant Microbe Interact* **32**, 164901664 (2019).

29. Jumper, J. *et al.* Highly accurate protein structure prediction with AlphaFold. *Nature* **596**, 583-589 (2021).

30. Greenfield, N.J. Using circular dichroism spectra to estimate protein secondary structure. *Nat Protoc* **1**, 2876-90 (2006).

31. Holzwarth, G.M. & Doty, P. The ultraviolet circular dichroism of polypeptides. *J Am Chem Soc.* **87**, 218-228 (1965).

32. Velivelli, S.L. *et al.* Antifungal symbiotic peptide NCR044 exhibits unique structure and multi-faceted mechanisms of action that confer plant protection. *PNAS* **117,** 16043-16054 (2020).

33. Bi, K. *et al.* The *Botrytis cinerea* Crh1 transglycosylase is a cytoplasmic effector triggering plant cell death and defense response. *Nat Commun* **12**, 2166 (2021).

34. Shi, Z., Olson, C.A. & Kallenbach, N.R. Cation-pi interaction in model alpha-helical peptides. *J Am Chem Soc* **124**, 3284-91 (2002).

35. Schibli, D.J., Epand, R.F., Vogel, H.J. & Epand, R.M. Tryptophan-rich antimicrobial peptides: comparative properties and membrane interactions. *Biochem Cell Biol* **80**, 667-77 (2002).

36. Falanga, A. *et al.* Cyclic peptides as novel therapeutic microbicides: Engineering of human defensin mimetics. *Molecules* **22**(2017).

37. Lopes, J.L., Miles, A.J., Whitmore, L. & Wallace, B.A. Distinct circular dichroism spectroscopic signatures of polyproline II and unordered secondary structures: applications in secondary structure analyses. *Protein Sci* **23**, 1765-72 (2014).

38. Spelbrink, R.G. *et al.* Differential antifungal and calcium channel-blocking activity among structurally related plant defensins. *Plant Physiol* **135**, 2055-67 (2004).

39. Terras, F.R. *et al.* Analysis of two novel classes of plant antifungal proteins from radish (*Raphanus sativus* L.) seeds. *J Biol Chem* **267**, 15301-9 (1992).

40. Munoz, A., Marcos, J.F. & Read, N.D. Concentration-dependent mechanisms of cell penetration and killing by the *de novo* designed antifungal hexapeptide PAF26. *Mol Microbiol* **85**, 89-106 (2012).

41. Schwinges, P. *et al.* A bifunctional dermaseptin-thanantin dipeptide functionalizes the crop surface for sustainable pest management. *Green Chemistry* **21**, 2316 (2019).

42. Shafee, T.M. & Anderson, M.A. A quantitative map of protein sequence space for the cis-defensin superfamily. *Bioinformatics* **35**, 743-752 (2019).

43. Liang, J. et al. Antifungal polypeptide from alfalfa and methods for controlling plant pathogenic fungi. US Patent 6,316,407 B1 (Monsanto Company, USA) (2001).

44. Chadha, S. & Kale, S.P. Simple fluorescence-based high throughput cell viability assay for filamentous fungi. *Lett Appl Microbiol* **61**, 238-44 (2015).

45. Zhang, N. *et al.* Comparative phenotyping of two commonly used *Chlamydomonas reinhardtii* background strains: CC-1690 (21gr) and CC-5325 (The CLiP Mutant Library Background). *Plants (Basel)* **11,** 585 (2022).

Acknowledgements

This work was supported, in part, by the National Science Foundation-EAGER grant IOS:1955461 awarded to D.S. We acknowledge imaging support from the Advanced Bioimaging Laboratory (RRID:SCR_018951) at the Danforth Plant Science Center and usage of the Leica SP8-X confocal microscope acquired through an NSF Major Research Instrumentation grant (DBI-1337680) and usage of the ZEISS Elyra 7 Super-Resolution Microscope acquired through an NSF Major Research Instrumentation grant (DBI-2018962).

Author contributions

M.T., H.L, C.Z. and D.S. conceived the research. M.T., H.L., A.D., K.C., G.B. and D.S. designed the research. M.T., H.L., A.D., G.B. and C.Z. conducted the experiments. M.T., H.L., A.D., C.Z., G.B., and D.S. analyzed and interpreted the results. M.T., H.L, G.B. C.Z. and D.S. wrote the manuscript.

Competing interests

M.T. and D.S. are listed as inventors in a related patent application. The remaining authors declare no competing interests.

Figure Legends

Figure 1. Amino acid sequences and structural analysis of MtDef4-derived GMA4CG_WT and its variants A. Amino acid sequence, net charge, and percentage of hydrophobic residues for GMA4CG_WT and its variants. The amino acid sequence of MtDef4 is shown on top with its γ-core motif highlighted by a red rectangle. The amino acid substitutions in GMA4CG_WT are shown in red box. Disulfide bonds verified in GMA4CG_V3 and GMA4CG_V6 are shown with a link. Z indicates the unnatural amino acid 2, 4-diaminobutyric acid. **B.** The antifungal activity of MtDef4, GMA4CG and its variants against *B. cinerea* in absence and presence of cations, and *F. graminearum* in absence of cations. MIC (Minimum Inhibitory Concentration) of each peptide was determined by resazurin assay. SFM (Synthetic Fungal Medium) is a low salt medium used in this study. **C.** Ribbon representations of the predicted structures of GMA4CG_WT and GMA4CG_V6 generated using AlphaFold2 and solvent accessible surface potential representations of these models generated using PyMol software. The disulfide bond of GMA4CG_V6 (C4-C17) is shown in yellow. The charges on the peptides surface are analyzed based on a dielectric constant of ±5. The white surface regions represent zero net charge, and the blue and red color surfaces indicate cationic and anionic regions, respectively. **D.** CD spectra of GMA4CG_WT (red) and GMA4CG_V6 (blue).

Figure 2. Topical application of GMA4CG_WT and its variants on detached *N. benthamiana* leaves confers resistance to gray mold. A. Scheme for application of GMA4CG_WT and GMA4CG_V1-V5 on tobacco leaves. Gray mold lesions on *N. benthamiana* leaves were observed and photographed at 48 hpi. The white light and CropRepoter images of the leaves are shown. **B.** Box & wishker's plots were used to represent the quantification of lesion sizes. **C**. Scheme for application of GMA4CG_V4 and GMA4CG_V6 on *N. benthamiana* leaves. The white light and CropReporter images of the infected leaves are shown. **D**. Box & wishker's plots were used to represent the quantification of lesion sizes. In **B** & **D**, the horizontal lines represent the median and

boxes indicate the 25th and 75th percentiles. One-Way Analysis of Variance (ANOVA) was used to determine statistical difference in lesion sizes between control (*B. cinerea*) and peptides. Three technical replications of tobacco leaves (n = 3) were tested in three independent biological replications. Asterisks represent significant differences between different groups (*P ≤ 0.05 **P < 0.01, ***P < 0.001, ****P ≤ 0.0001) using Tukey's honestly significant difference test (HSD) for comparison of multiple groups.

Figure 3. GMA4CG_V6 permeabilizes cell membrane of *B. cinerea*. A. Confocal microscopy images of the SG uptake in *B. cinerea* spores and germlings treated with 1.5 µM of GMA4CG_V6 for 30 min. Spores and germlings treated with H_2O served as controls. Scale bars= 20 µm. **B.** Representative images showing SG signals in *B. cinerea* spores treated with 1.5, 3, and 6 µM of GMA4CG_V6 for 1 h with no salt, for 1 h and 5 h with 100 mM KCl. The outline of each spore was highlighted using white imaginary line. Scale bar = 20 µm. The permeabilization rate (%) of each treatment was labeled on images. **C.** Quantitative measurements of cell membrane permeability in terms of fluorescence emitted by *B. cinerea* germlings treated with various concentrations of MtDef4, GMA4CG_WT and GMA4CG_V6 with and without 100 mM KCl. Membrane permeabilization increased with the increasing concentration of each peptide. Values are means of two biological replications. Error bars indicate standard deviations. Fluorescence measurements were taken at every 1 h for 5 h and the data were subsequently plotted.

Figure 4. Internalization of GMA4CG_V6 into *B. cinerea*. A. Time-lapse confocal microscopy images of *B. cinerea* show internalization of 1.5 µM of TMR-GMA4CG_V6 over time (T in min). Images were captured every 4 min starting from 3 min. Arrows indicate vacuole areas. Scale bars= 10 µm. **B.** Individual fluorescent (CMAC, TMR and FM4-64), and channel merged images of *B. cinerea* germlings treated with GMA4CG_V6 for 30 min. The overlap signal of CMAC and TMR, or TMR and FM4-64 is shown as white pixels. The threshold for each channel was 50% and for background was 20%. Scale bars= 10 µm. **C.** The fluorescent signal intensity of the ROI in B. Black arrows indicated the TMR-GMA4CG_V6 and FM4-64 signals overlapped at membrane and the red arrows indicated the TMR-GMA4CG_V6 and CMAC signals overlapped at the vacuole. **D.** Individual fluorescent (TMR and FM4-64) and channel merged images of *B. cinerea* germlings treated with TMR-GMA4CG_V6 for 60 min. The overlap signal of TMR and FM4-64 is shown as white pixels. The threshold for each channel was 50% and for background was 20%. Scale bars= 10 µm. **E.** The fluorescent signal intensity of the ROI in D. The red arrow indicated the vacuole localization of TMR-GMA4CG_V6 and the green arrow indicated the FM4-64 in the cytoplasm. In the cytoplasm, increased signal intensity of TMR-GMA4CG_V6 was observed. **F.** Cell surface fluorescence showed in 2.5D. The vertical direction indicated the fluorescence intensity of each pixel, and the taller peaks represent greater fluorescence intensity. The corresponding 2D images are shown on the left bottom. **G.** Box plot for cell surface fluorescence quantification. Total fluorescence intensity of each cell was normalized to the cell perimeter length. The lower threshold was set to 7000 to substrate the signal in cytoplasm. Statistical analyses were performed using a two-tailed t-test assuming unequal variance. P-value over 0.05 indicated no significant difference and less than 0.05 indicates a significant difference. n= 24-39.

Figure 5. **GMA4CG_V6 exhibits preventative and curative antifungal activity against gray mold in *N. benthamiana* plants A.** Preventative activity of GMA4CG_V6. Four-week-old *N. benthamiana* plants were sprayed with either 2 mL water or peptide (GMA4CG_WT or GMA4CG_V6) at 12 µM or 24 µM concentrations prior to spray-inoculation with 1 mL of 8×10^4 spores per mL of *B. cinerea* fresh spore suspension. The mock plants were only sprayed with water

(no fungal spore suspension). The CropReporter images of plants were taken 72 hpi. Maximum quantum yield of PSII photochemistry (Fv/Fm) was determined at 72 hpi. Red color represents class I, low photosynthesis efficiency attributed to extensive tissue damage. Green color indicates class V, high photosynthesis efficiency. **B.** The calculated photosynthetic quantum yield (Fv/Fm) for individual *N. benthamiana* plants. **C.** Curative antifungal activity of GMA4C_V6. Four-week-old *N. benthamiana* plants were first spray-inoculated using 1 mL of 8×10^4 *B. cinerea* spore suspension. At 2, 15, or 30 h post-inoculation, plants were sprayed with 2 mL of peptide (GMA4CG_WT or GMA4CG_V6) at a concentration of 12 µM or water. The mock plants were only sprayed with water (no fungal spore suspension). Maximum quantum yield was determined as described above. **D.** The calculated photosynthetic quantum yield (Fv/Fm) for individual *N. benthamiana* plants. In **B** and **D**, the horizontal lines represent the median and boxes indicate the 25th and 75th percentiles. One-Way Analysis of Variance (ANOVA) was used to determine statistical difference between control (*B. cinerea* alone), mock (water alone), and peptide-treated inoculated plants. Each technical replication included four plants (n=4). Three biological replications were performed. Asterisks represent significant differences between different groups with P values ($^{ns}P > 0.05$, $*P \leq 0.05$ $**P \leq 0.01$, $****P \leq 0.0001$) determined using Tukey's honestly significant difference test (HSD) for comparison of multiple groups.

Figure 6. **GMA4CG_V6 exhibits curative antifungal activity against gray mold in tomato plants. A.** Three-week-old tomato plants were spray-inoculated with 1 mL of 8×10^4 *B. cinerea* spore suspension. At 12 h post-inoculation, plants were sprayed with 2 ml water or 2 ml peptide (GMA4CG_WT or GMA4CG_V6) at concentration of 6, 12, or 24 µM. The CropReporter images of the plants were taken 72 hpi and the maximum quantum yield of PSII photochemistry (Fv/Fm) was determined. Red color represents class I, low efficiency photosynthesis attributed to extensive tissue damage. Green color represents class V, high efficiency photosynthesis. **B.** The calculated photosynthetic quantum yield (Fv/Fm) for individual tomato plants. The horizontal lines represent the median and boxes indicate the 25th and 75th percentiles. One-Way Analysis of Variance (ANOVA) was used to determine statistical difference between control (*B. cinerea* alone), mock (water alone), and peptide-treated inoculated plants. Each technical replication included four plants (n= 4). Three biological replications were performed. Asterisks represent significant differences between different groups with P values ($^{ns}P > 0.05$, $*P \leq 0.05$ $**P < 0.01$, $****P \leq 0.0001$) determined using Tukey's honestly significant difference test (HSD) for comparison of multiple groups. **C.** Germination and growth of *B. cinerea* spores on the tomato leaf surfaces in presence of GMA4CG_V6 or water. Tomato plants were inoculated with *B. cinerea* spores. Infection was allowed to progress for 12 h and then the plants were sprayed with water or with GMA4CG_V6. Forty-eight h post peptide or water treatment, leaf samples were fixed in 4% paraformaldehyde and stained with CFW for 30 min. ZEISS Axio ZoomV16 was used to capture images. Arrowheads point to the germinated hyphae of *B. cinerea*.

Figure 7. A proposed model for the modes of antifungal action of GMA4CG_V6 against *B. cinerea*. GMA4CG_V6 sprayed on *B. cinerea* infected leaves first binds to the pathogen's cell walls and the peptide starts to permeabilize the fungal plasma membrane. Binding to plasma membrane-resident phosphoinositides presumably plays a role in membrane permeabilization. At low concentration, GMA4CG_V6 is internalized into cell vacuoles through ATP-dependent endocytic mechanisms. At high concentration, GMA4CG_V6 targets the cytoplasm immediately following cell entry. Cell death occurs only after GMA4CG_V6 diffuses into the cytoplasm and not while in the vacuole. N: nucleus, V: vacuole, E: endosome.

Figure 1

A

MtDef4: RTCESQSHKFKGPCASDHNCASVCQTERFSGGRCRGFRRRCFCTTHC

	Sequences	Net charge	% hydrophobic amino acids
GMA4CG_WT:	GGRCRGFRRRCFCTTHC	4.9	11.8
GMA4CG_V1:	GGRCKGFRRRCFCTRIC	5.8	17.7
GMA4CG_V2:	GGRCRGFRRRCFCTRIC	5.8	17.7
GMA4CG_V3:	GGRCKGFRRRVFVTRIC	5.9	29.4
GMA4CG_V4:	FGRCRGFRRRCFCWRWC	5.8	29.4
GMA4CG_V5*:	FGZCZGFZZZCFCWZWC	5.8	29.4
GMA4CG_V6:	GGRCKGFRRRWFWTRIC	5.9	29.4

B

	B.cinerea (MIC) µM				*F.graminearum* (MIC) µM
Peptide	SFM	SFM+100 mM NaCl	SFM+100 mM KCl	SFM+2 mM $CaCl_2$	SFM
MtDef4	0.75	> 6	> 6	> 6	0.75
GMA4CG_WT	3	3	6	6	3
GMA4CG_V1	3	1.5	3	3-6	3
GMA4CG_V2	6	3	6	6	6
GMA4CG_V3	3	1.5-3	> 6	> 6	3
GMA4CG_V4	1.5-3	1.5	1.5	3	1.5-3
GMA4CG_V5	3-6	6	> 6	> 6	3
GMA4CG_V6	1.5	1.5	1.5-3	3	1.5

C

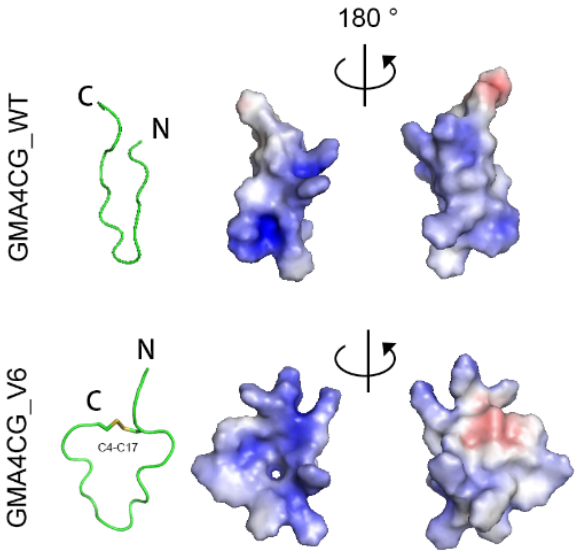

D

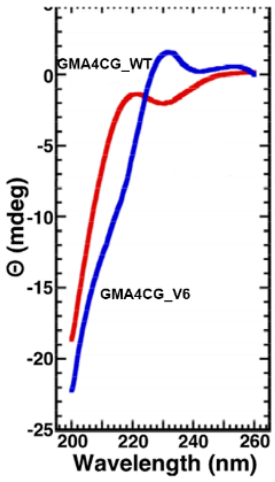

Figure 2

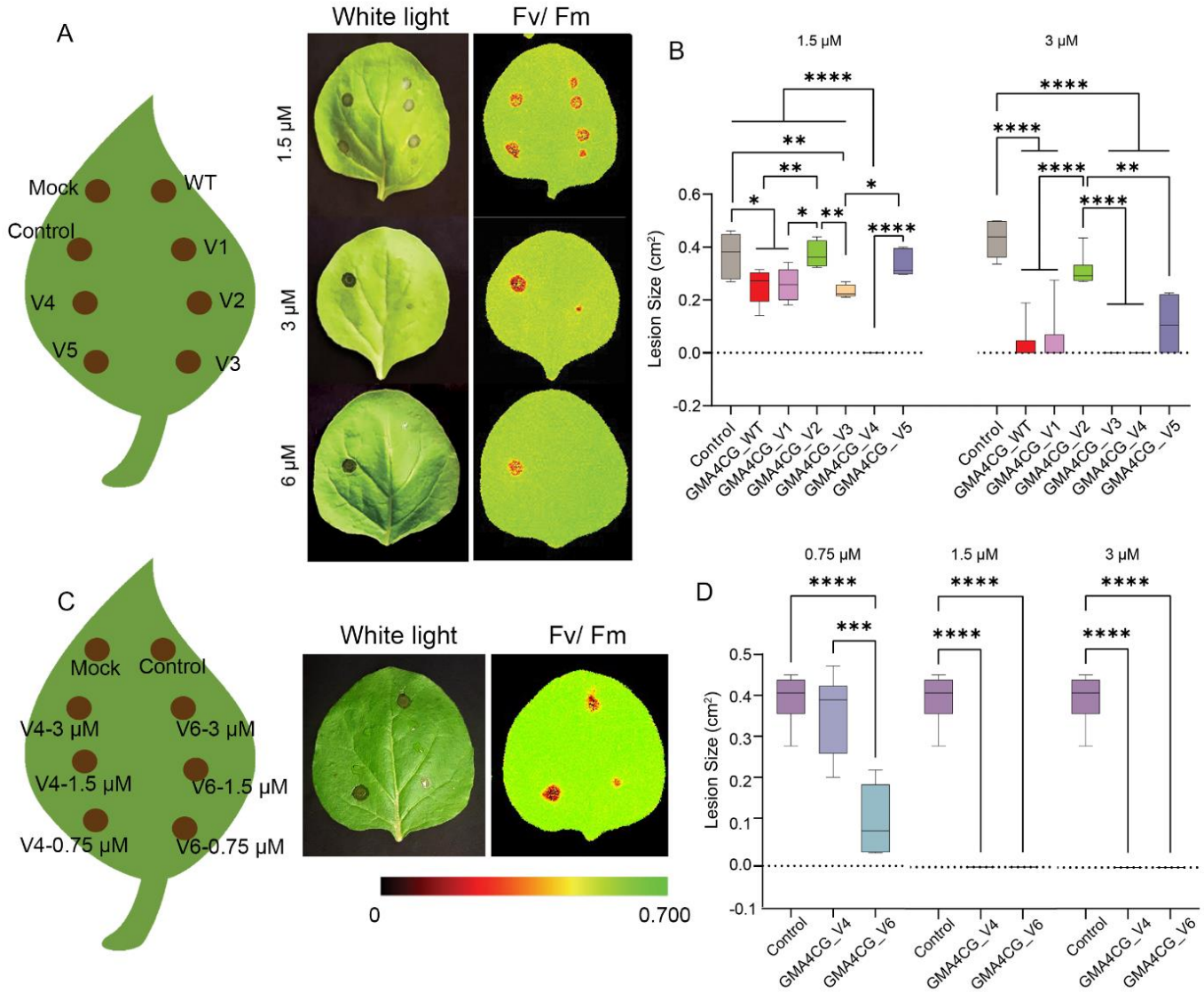
A
Mock
WT
Control
V1
V4
V2
V5
V3
White light
Fv/ Fm
1.5 µM
3 µM
6 µM
B
1.5 µM
3 µM
Lesion Size (cm²)
Control
GMA4CG_WT
GMA4CG_V1
GMA4CG_V2
GMA4CG_V3
GMA4CG_V4
GMA4CG_V5
C
Mock
Control
V4-3 µM
V6-3 µM
V4-1.5 µM
V6-1.5 µM
V4-0.75 µM
V6-0.75 µM
White light
Fv/ Fm
0
0.700
D
0.75 µM
1.5 µM
3 µM
Lesion Size (cm²)
Control
GMA4CG_V4
GMA4CG_V6

Figure 3

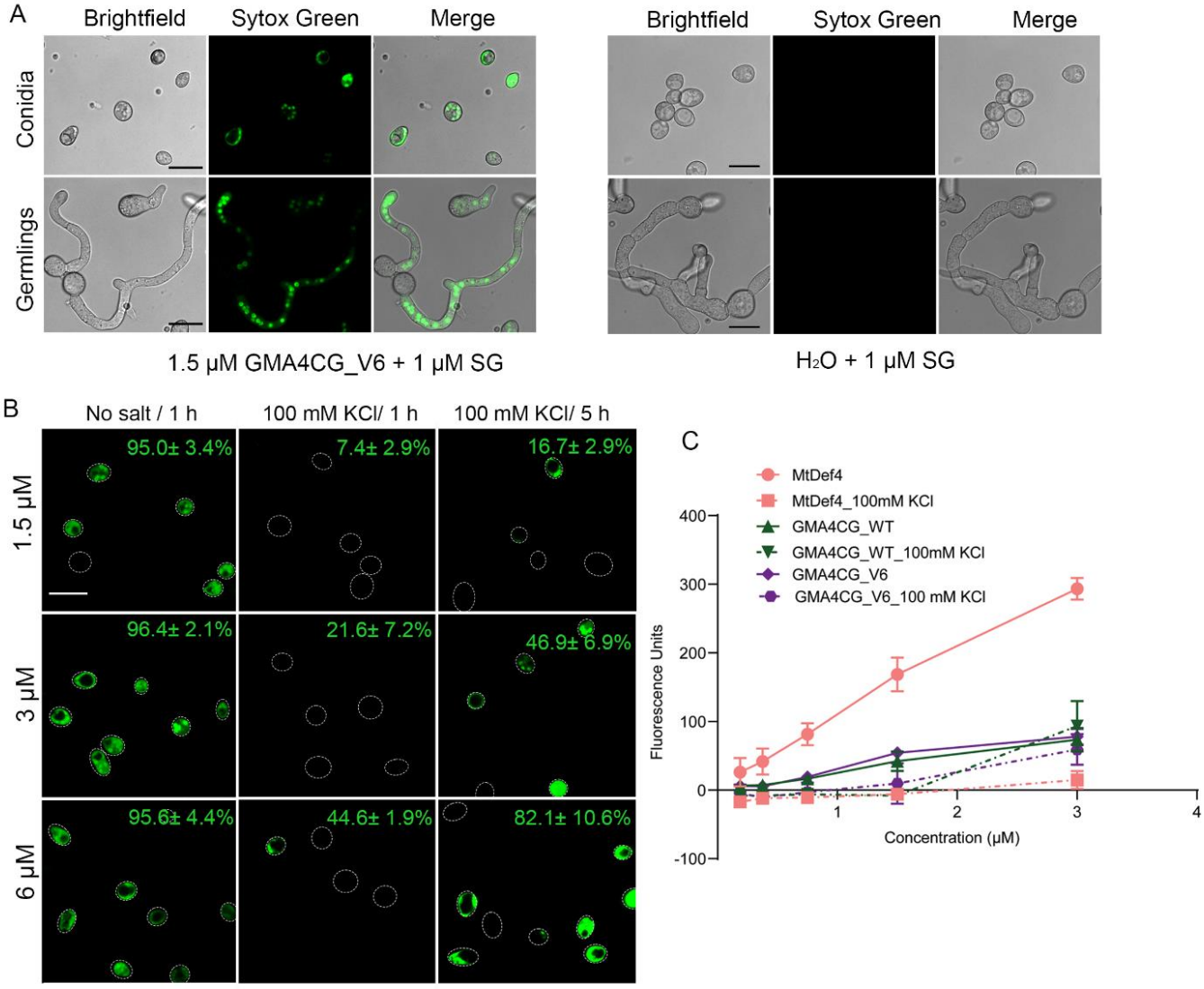
A
Brightfield
Sytox Green
Merge
Conidia
Germlings
1.5 µM GMA4CG_V6 + 1 µM SG
Brightfield
Sytox Green
Merge
H2O + 1 µM SG
B
No salt / 1 h
100 mM KCl/ 1 h
100 mM KCl/ 5 h
1.5 µM
3 µM
6 µM
95.0± 3.4%
7.4± 2.9%
16.7± 2.9%
96.4± 2.1%
21.6± 7.2%
46.9± 6.9%
95.6± 4.4%
44.6± 1.9%
82.1± 10.6%
C
MtDef4
MtDef4_100mM KCl
GMA4CG_WT
GMA4CG_WT_100mM KCl
GMA4CG_V6
GMA4CG_V6_100 mM KCl
Fluorescence Units
400
300
200
100
0
-100
1
2
3
4
Concentration (µM)

Figure 4

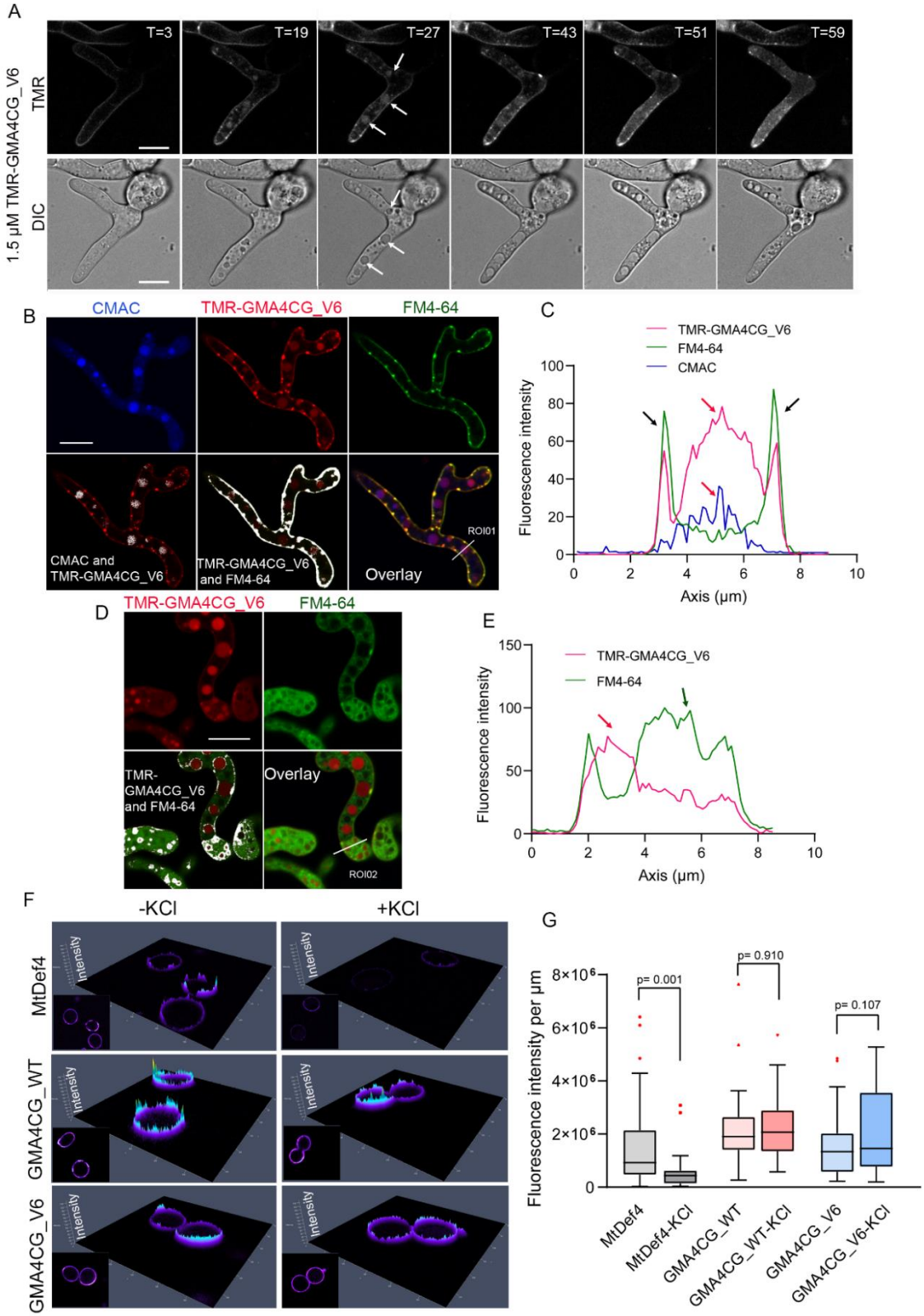
A
1.5 µM TMR-GMA4CG_V6
TMR
DIC
T=3
T=19
T=27
T=43
T=51
T=59
B
CMAC
TMR-GMA4CG_V6
FM4-64
CMAC and TMR-GMA4CG_V6
TMR-GMA4CG_V6 and FM4-64
Overlay
ROI01
C
TMR-GMA4CG_V6
FM4-64
CMAC
Fluorescence intensity
Axis (µm)
D
TMR-GMA4CG_V6
FM4-64
TMR-GMA4CG_V6 and FM4-64
Overlay
ROI02
E
TMR-GMA4CG_V6
FM4-64
Fluorescence intensity
Axis (µm)
F
-KCl
+KCl
MtDef4
GMA4CG_WT
GMA4CG_V6
Intensity
G
Fluorescence intensity per µm
p= 0.001
p= 0.910
p= 0.107
MtDef4
MtDef4-KCl
GMA4CG_WT
GMA4CG_WT-KCl
GMA4CG_V6
GMA4CG_V6-KCl

Figure 5

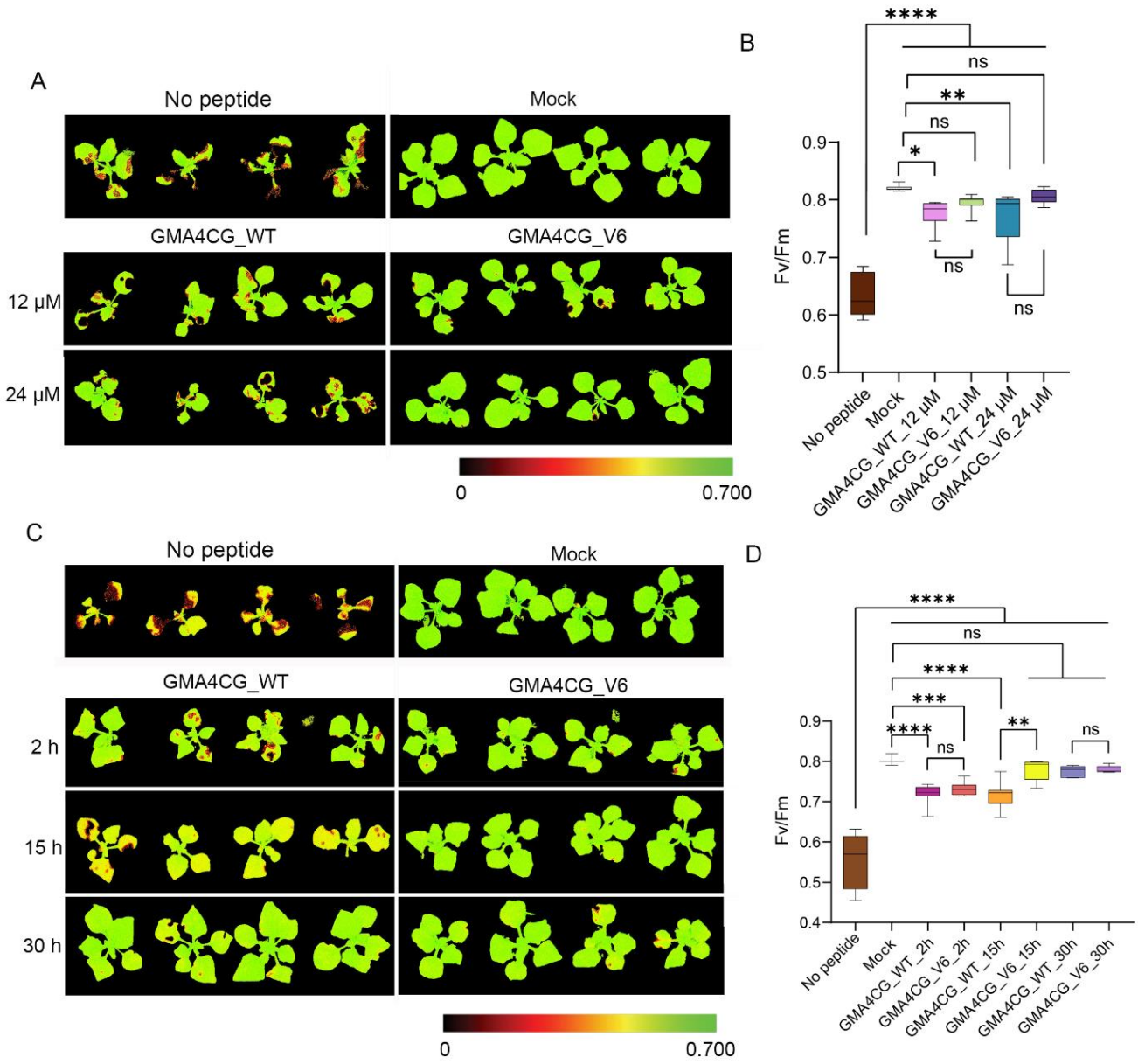
A
No peptide
Mock
GMA4CG_WT
GMA4CG_V6
12 µM
24 µM
0
0.700
B
****
ns
**
ns
*
ns
ns
Fv/Fm
0.9
0.8
0.7
0.6
0.5
No peptide
Mock
GMA4CG_WT_12 µM
GMA4CG_V6_12 µM
GMA4CG_WT_24 µM
GMA4CG_V6_24 µM
C
No peptide
Mock
GMA4CG_WT
GMA4CG_V6
2 h
15 h
30 h
0
0.700
D
****
ns
****
***
****
ns
**
ns
Fv/Fm
0.9
0.8
0.7
0.6
0.5
0.4
No peptide
Mock
GMA4CG_WT_2h
GMA4CG_V6_2h
GMA4CG_WT_15h
GMA4CG_V6_15h
GMA4CG_WT_30h
GMA4CG_V6_30h

Figure 6

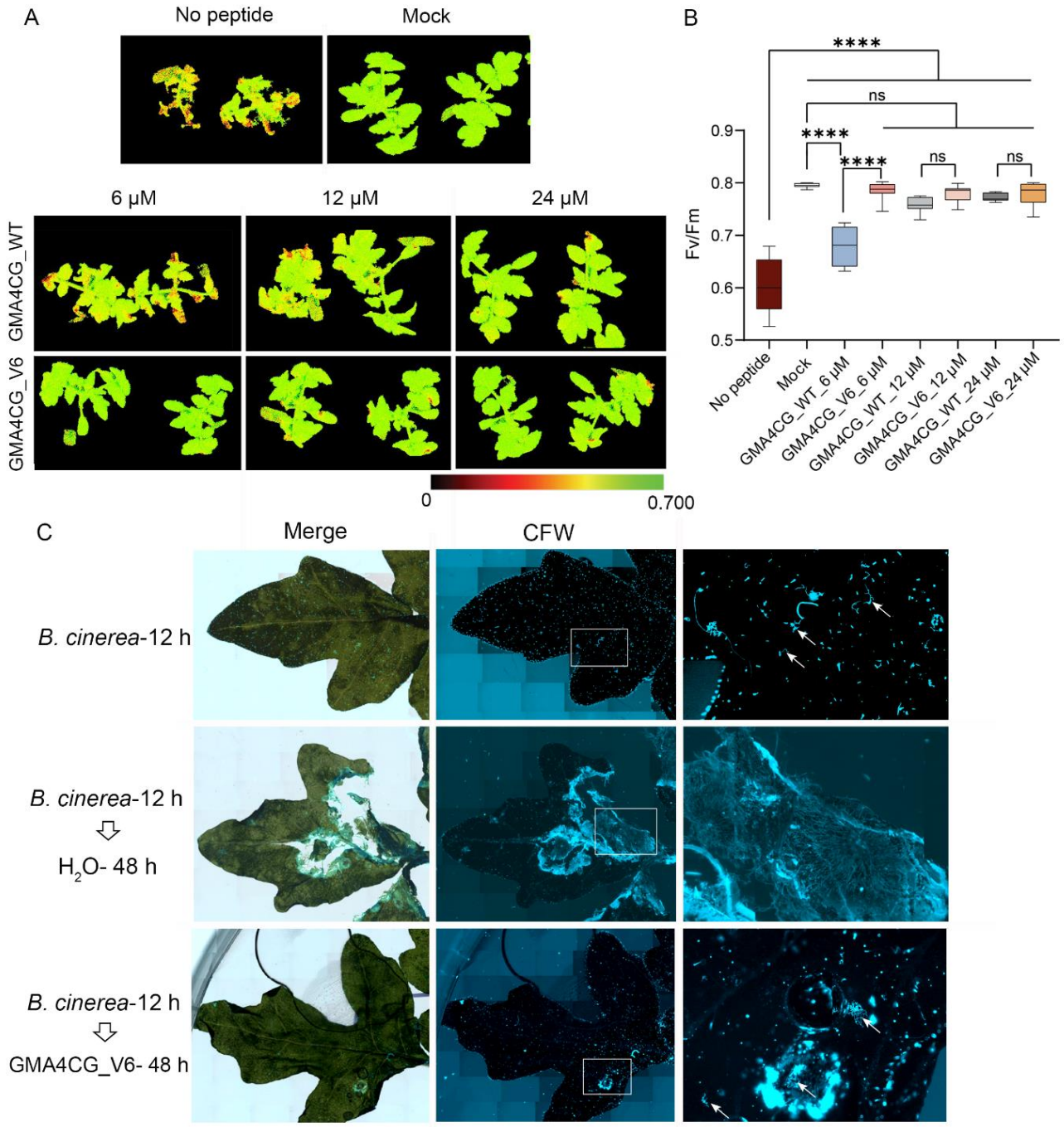
A
No peptide
Mock
6 µM
12 µM
24 µM
GMA4CG_WT
GMA4CG_V6
0
0.700
B
****
ns
****
****
ns
ns
Fv/Fm
0.9
0.8
0.7
0.6
0.5
No peptide
Mock
GMA4CG_WT_6 µM
GMA4CG_V6_6 µM
GMA4CG_WT_12 µM
GMA4CG_V6_12 µM
GMA4CG_WT_24 µM
GMA4CG_V6_24 µM
C
Merge
CFW
B. cinerea-12 h
B. cinerea-12 h
H2O- 48 h
B. cinerea-12 h
GMA4CG_V6- 48 h

Figure 7

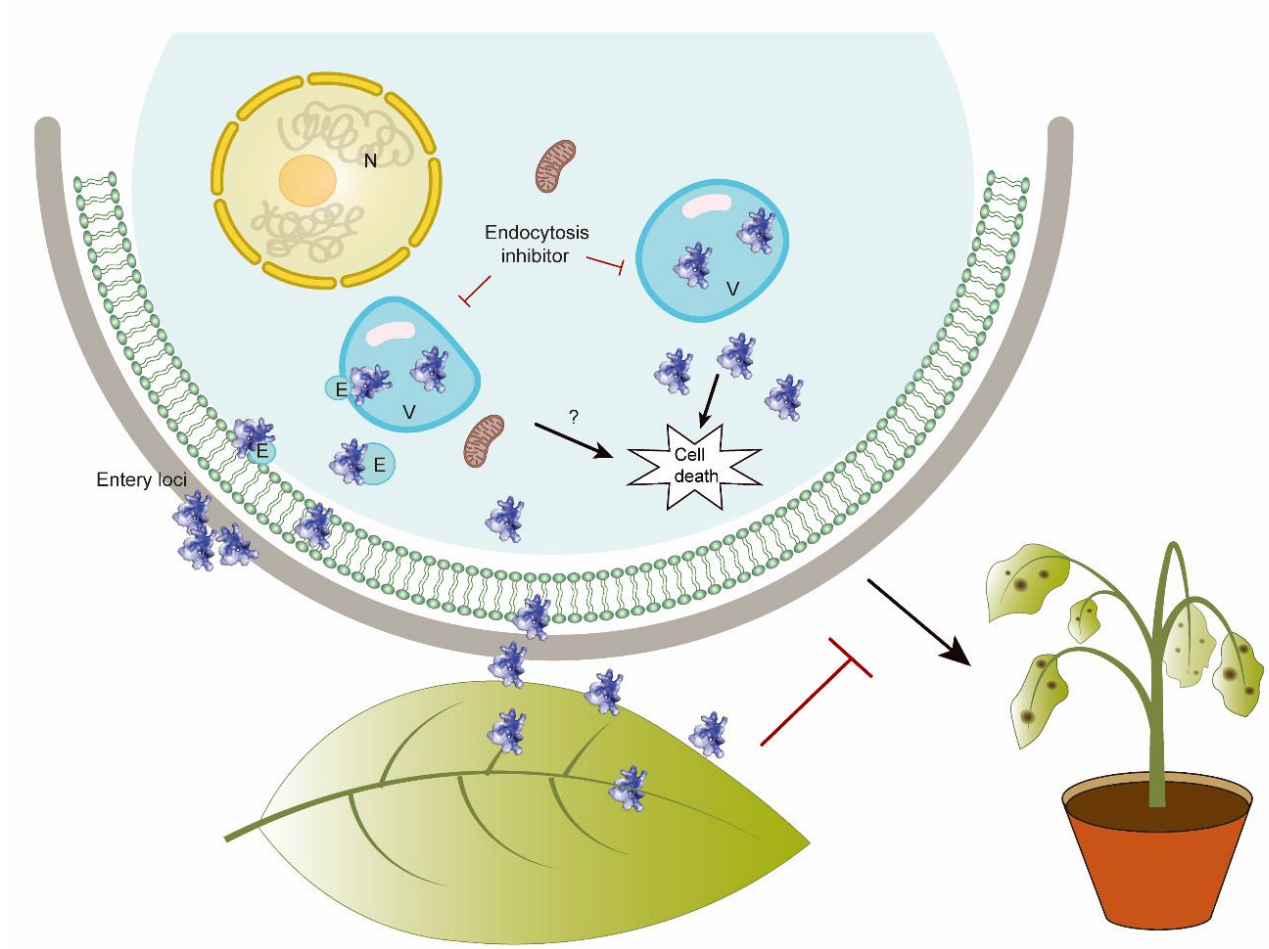

Table 1. MIC values of the linear GMA4CG_V6 and its alanine scanning variants against *B. cinerea*			
Peptide	**Sequence**	**SFM (MIC) µM**	**SFM+100 mM NaCl (MIC) µM**
GMA4CG_V6	GGRCKGFRRRWFWTRIC	1.5	1.5
GMA4CG_V6_Ala1	**AAAA**KGFRRRWFWTRIC	6	6
GMA4CG_V6_Ala2	GGRC**AAA**RRRWFWTRIC	6	6
GMA4CG_V6_Ala3	GGRCKGF**AAAA**FWTRIC	12	24
GMA4CG_V6_Ala4	GGRCKGFRRRW**AAA**RIC	6	6
GMA4CG_V6_Ala5	GGRCKGFRRRWFWT**AAA**	6	6